

Surface-Nitrogen Removal in a Steady-State NO + H₂ Reaction on Pd(110)

Yunsheng Ma and Tatsuo Matsushima*

Catalysis Research Center, Hokkaido University, Sapporo 001-0021, Japan

Received: August 26, 2004; In Final Form: October 16, 2004

Surface-nitrogen removal steps were analyzed in the course of a catalyzed NO + H₂ reaction on Pd(110) by angle-resolved mass spectroscopy combined with cross-correlation time-of-flight techniques. Four removal steps, i.e., (i) the associative process of nitrogen atoms, 2N(a) → N₂(g), (ii) the decomposition of the intermediate, NO(a) + N(a) → N₂O(a) → N₂(g) + O(a), (iii) its desorption, N₂O(a) → N₂O(g), and (iv) the desorption as ammonia, N(a) + 3H(a) → NH₃(g), are operative in a comparable order. Above 600 K, process (i) is predominant, whereas the others largely contribute below 600 K. Process (iv) becomes significant at H₂ pressures above a critical value, about half the NO pressure. Hydrogen was a stronger reagent than CO toward NO reduction and relatively enhanced the N(a) associative process.

I. Introduction

The NO reduction by CO, H₂, and hydrocarbon on rhodium and palladium surfaces has received much attention because of its importance in controlling automobile exhaust gas.¹ In this catalytic reduction, N₂O is concomitantly produced as one of the undesired byproducts. N₂O itself is harmful and has a remarkable greenhouse effect. In the NO + H₂ reaction, another undesired product, NH₃, is formed. Therefore, it is necessary to improve the selectivity to N₂ in these catalytic processes; however, knowledge of the reaction mechanism is still limited, especially regarding the steps for the removal of surface nitrogen. These are difficult to analyze because of the presence of several rapid pathways after the slow NO dissociation. This paper contains the first confirmation that the N₂O intermediate decomposition is the final step of the main pathway in a steady-state NO + H₂ reaction on Pd(110).

Many publications have dealt with the NO + H₂ reaction on Pt, Rh, and Pt–Rh alloy surfaces.^{2–8} However, most of them have focused on the nonlinear behavior of surface reactions, in which the removal of surface nitrogen was tacitly assumed to be rapid enough not to play a rate-limiting role. Ikai et al. found that, in the course of heating in their angle-resolved (AR) temperature-programmed reaction (TPR) of NO and H₂ or CO on Pd(110), the N₂ peak at 490 K involved desorption collimated at 38° off normal toward the [001] direction and desorbing N₂ in the other peak at around 600 K collimated at the surface normal, whereas the off-normal peak at 490 K was absent in the subsequent cooling.⁸ Furthermore, they confirmed that the reaction between ¹⁴N(a) and ¹⁵NO(a) emitted the product ¹⁴N¹⁵N in an inclined way, while the associative nitrogen desorption collimated along the surface normal. The authors argued that the inclined N₂ desorption originated in the desorption-mediated reaction without the formation of the intermediate N₂O. On the other hand, our previous study revealed that desorbing N₂ from N₂O dissociation, NO decomposition, and a steady-state NO + CO reaction on Pd(110) commonly showed identical angular and velocity distributions.^{9–12} Thus, N₂O(a) was proposed to be oriented along the [001] direction before dissociation. This

structure was later confirmed by density functional theory (DFT) calculations and near-edge X-ray absorption fine structure (NEXAFS) and scanning tunneling microscopy (STM) work.^{13–15}

This peculiar N₂ desorption is useful to analyze the pathway of the removal of surface nitrogen because the associative desorption of N(a) emits N₂ sharply along the surface normal.^{8,16} Furthermore, the angular distribution is always related to the product desorption step whenever any step becomes rate-determining.^{17,18} The angular and velocity distributions of desorbing products in the NO decomposition have been analyzed with several relaxation methods, such as modulated molecular beams¹⁹ and AR-TPR.^{8–11,20–22} Steady-state conditions, however, could not be established for the reaction, and then simple phenomena were not differentiated from kinetic behavior under steady-state conditions.^{8,22} In the present work, AR product desorption measurements were successfully performed for a steady-state NO + H₂ reaction.

II. Experiments

The apparatus has three separately pumped chambers.^{17,23} The reaction chamber is equipped with reverse-view low-energy electron diffraction (LEED) and X-ray photoelectron spectroscopy (XPS) optics, an ion gun, and a quadrupole mass spectrometer (QMS) for angle-integrated (AI) measurements. The chopper house, which has a large pumping rate of about 7 m³·s⁻¹ for a high angle resolution,²⁴ has a narrow slit facing the reaction chamber and a cross-correlation random chopper blade. Another QMS was used in the analyzer connected through a narrow tube for AR product desorption and time-of-flight analyses. The distance from the ionizer to the chopper blade was 377 mm, and the time resolution was selected at 20 μs.

¹⁵NO was introduced through a doser with a small orifice (diameter 0.1 mm) about 2 cm from a sample crystal while D₂ or CO was backfilled. The product ¹⁵N₂, ¹⁵ND₃, D₂O, and ¹⁵N₂O signals were monitored in both AI and AR forms. Hereafter, these are simply described as N₂, ND₃, D₂O, and N₂O in the text. The desorption angle (polar angle, θ) was scanned in the plane along the [001] direction.¹⁷ The N₂ signals in both QMSs were corrected by the contribution due to the fragmentation of N₂O. The pressures of reactant gases were also corrected by their mass spectrometer sensitivities.

* To whom correspondence should be addressed. Fax: +81-11-706-9120. E-mail: tatmatsu@cat.hokudai.ac.jp.

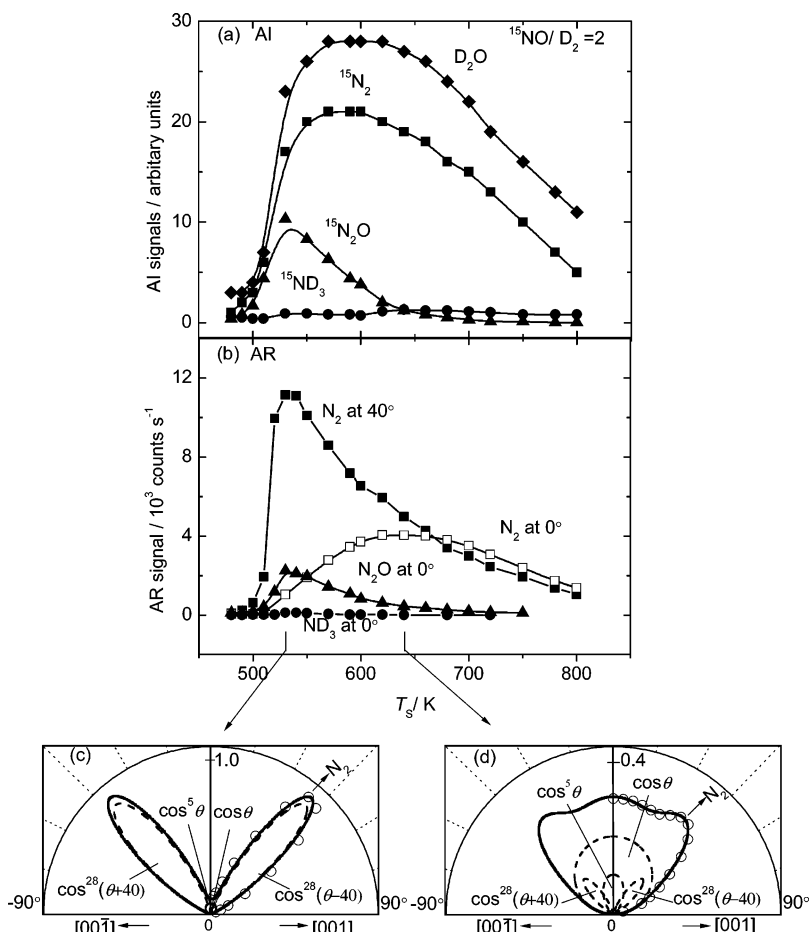


Figure 1. T_S dependence of (a) AI and (b) AR signals of products at the collimation positions in a steady-state $^{15}\text{NO} + \text{D}_2$ reaction at $P_{\text{NO}} = 5 \times 10^{-6}$ Torr with the pressure ratio $^{15}\text{NO}/\text{D}_2 = 2$. Angular distributions of desorbing $^{15}\text{N}_2$ at (c) 530 K and (d) 640 K. Typical deconvolutions shown by broken curves are based on the velocity distribution analysis. The ordinate was normalized to the maximum at 530 K.

III. Results

A. General Features. The AI signal was determined by the QMS in the reaction chamber as the difference in the signal between the desired surface temperature (T_S) and room temperature. The AI signals are shown for desorbing N_2 , N_2O , ND_3 , and D_2O at a fixed NO pressure of 5×10^{-6} Torr and the pressure ratio $P_{\text{NO}}/P_{\text{D}_2} = 2$ (Figure 1a). All the rates are negligible below 490 K, increase rapidly at around 510 K to a maximum with increasing T_S , and decrease again above 650 K. No hysteresis was found in their rates with decreasing T_S . With the pressure ratio $P_{\text{NO}}/P_{\text{D}_2} = 2$, ND_3 formation was negligible in the temperature range studied. In fact, ND_3 formation was observed only at higher P_{D_2} as described in the following section.

On the other hand, the AR signal was obtained by the QMS in the analyzer as the difference between the signal at the desired angle and that when the crystal was away from the line-of-sight position. The AR N_2 signals at $\theta = 0^\circ$ and 40° are displayed versus T_S because these are their collimation angles (Figure 1b). There are noticeable differences in their temperature dependence. The AR N_2 signal at 40° becomes noticeable at 500 K, increases quickly to the maximum at 530 K, and then begins to decrease above 550 K. On the other hand, the N_2 signal at $\theta = 0^\circ$ increases slowly above 500 K and reaches the maximum at around 640 K. This indicates remarkable changes in the angular distributions with increasing T_S . Both N_2 signals at different desorption angles were highly reduced at higher temperatures but still noticeable even at 800 K. It should be

noticed that the AR N_2O signal at $\theta = 0^\circ$ followed a T_S dependence similar to that of N_2 at $\theta = 40^\circ$.

Only the (1×1) pattern was observed in LEED measurements under a steady-state NO + D_2 reaction at the NO pressure of 5×10^{-8} Torr and $P_{\text{NO}}/P_{\text{D}_2} = 2$ in the range of $T_S = 450$ –800 K. This is very different from the results of the CO + O_2 reaction showing $c(2 \times 4)$ or $(1 \times n)$ structures.²⁵

B. Angular Distribution. Both N_2O and ND_3 desorption showed the cosine distribution characteristic of the desorption after thermalization to T_S . It was confirmed by the velocity distribution, which was fully described by a Maxwellian distribution at the surface temperature; i.e., N_2O and ND_3 were trapped on the surface before desorption. On the other hand, the angular distribution of desorbing N_2 changed significantly with increasing temperature. The results are shown in Figure 1c,d. At $T_S = 530$ K, N_2 desorption mostly collimated around 40° , while at 640 K (Figure 1d), the intensity of the N_2 signal at the normal direction increased. The distribution was deconvoluted into three components on the basis of the following velocity distribution analysis.

Typical velocity distribution curves at different desorption angles at $T_S = 640$ K are shown in Figure 2. The apparent translational temperature calculated from the average kinetic energy ($\langle E \rangle$) as $T_{\langle E \rangle} = \langle E \rangle / 2k$, is shown in angular brackets in the figure, where k is the Boltzmann constant. The value was maximized at around the collimation angle to the value of 2200 K at $T_S = 640$ K. It decreased quickly with an increasing shift from the collimation angle. This angle dependence was consistent with the inclined desorption. The velocity distribution

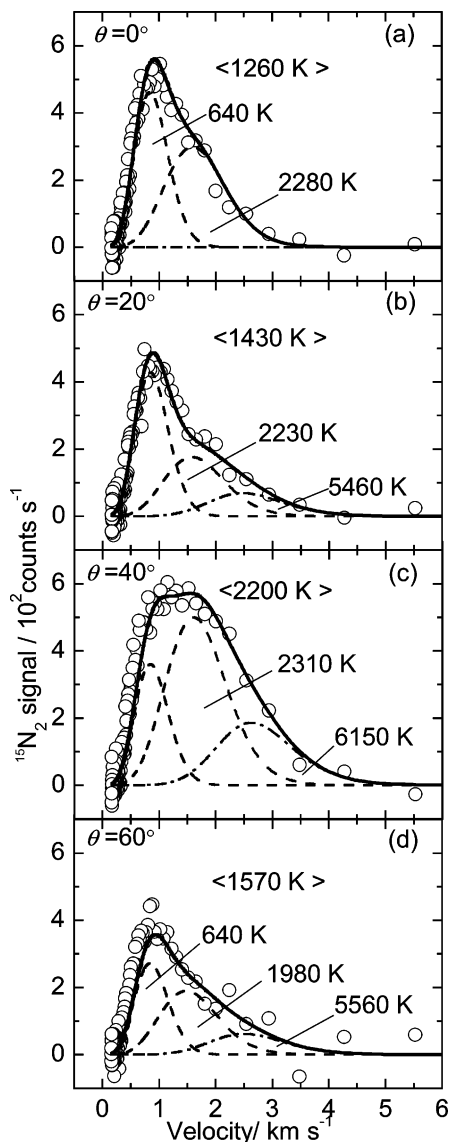


Figure 2. Velocity distributions of desorbing $^{15}\text{N}_2$ at different angles. The average kinetic energy is indicated within angular brackets in the temperature units. Typical deconvolutions (see the text) are drawn by broken curves. The solid line indicates their summation. The condition is at $T_s = 640\text{ K}$ in Figure 1.

involved components faster than those expected by the Maxwell distribution at the surface temperature of 640 K. The latter component was expected to follow the cosine distribution, and it was first subtracted from the velocity distribution curves. The resultant velocity curve provided the flux of the fast component, which peaked at $\theta = 0^\circ$ and 40° . The fast component with translational temperature about 3 times higher than the surface temperature was observed at the normal direction. On the other hand, the fast component at $\theta = 40^\circ$ reached the maximum with a translational temperature of about 3200 K.

Assuming a power series of the cosine of the desorption angle to each component, the N_2 distribution was in a two-directional form approximated as $\cos^{28}(\theta + 40) + \cos^{28}(\theta - 40)$ and the N_2 signal at the normal direction was very small below 600 K. The total signal at 530 K, for example, can be described as $0.95\{\cos^{28}(\theta + 40) + \cos^{28}(\theta - 40)\} + 0.03 \cos^5(\theta) + 0.07 \cos(\theta)$. At higher $T_s = 640\text{ K}$, the normally directed component was enhanced. The signal intensity at the normal direction increased with increasing T_s , indicating the presence of the normally directed fast component. The total signal at 640 K

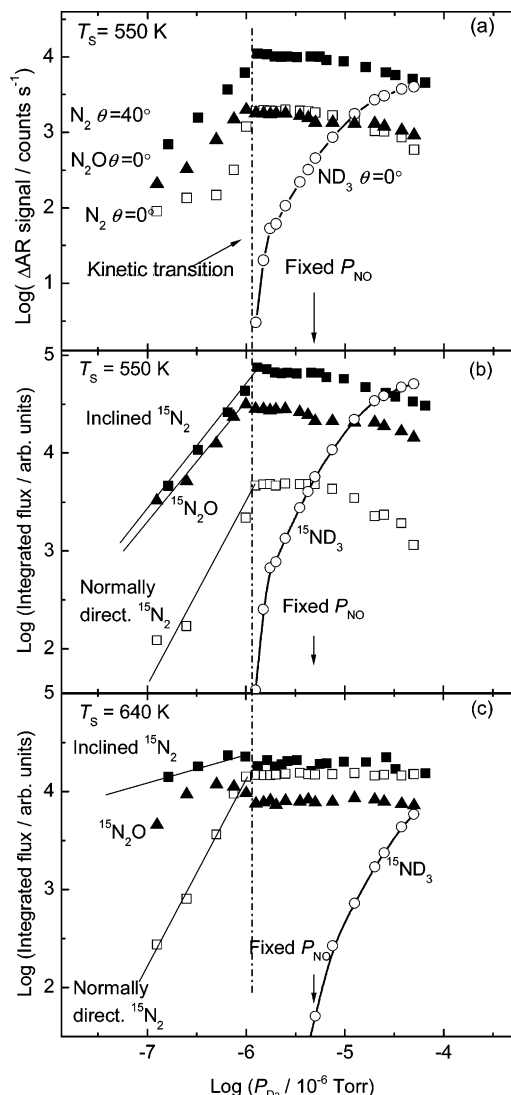


Figure 3. P_{D_2} dependence of each component formation at a fixed ^{15}NO pressure of $5 \times 10^{-6}\text{ Torr}$: (a) AR signals of different products at $T_s = 550\text{ K}$ and (b) component flux after integration, (c) component flux after integration at $T_s = 640\text{ K}$. The normally directed $^{15}\text{N}_2$ involved the cosine component. The vertical broken line indicates the kinetic transition point.

was approximated as $0.51 \cos \theta + 0.26 \cos^5 \theta + 0.3\{\cos^{28}(\theta + 40) + \cos^{28}(\theta - 40)\}$. The inclined N_2 desorption was due to N_2O decomposition, and the normally directed N_2 component comes from the associative desorption of $\text{N}(\text{a})$. These components showed different behavior toward the variation of the surface temperature and the pressures of D_2 and NO , which also suggests that they come from different nitrogen removal steps. The cosine component, however, cannot be assigned to a definite process from the angular distribution.

C. Hydrogen Effect. The product formation kinetics changed sharply at a critical D_2 pressure. The AR signals of different products in a steady-state $\text{NO} + \text{D}_2$ reaction at 550 K are displayed as a function of the deuterium pressure in Figure 3a, where the NO pressure was fixed at $5 \times 10^{-6}\text{ Torr}$. With increasing P_{D_2} , the AR N_2 signal at 40° increases, is maximized at $P_{\text{D}_2} = 1 \times 10^{-6}\text{ Torr}$, and slightly decreases above this level. Both the N_2 and N_2O signals at $\theta = 0^\circ$ also showed similar dependence. These AR signals were integrated around their collimation angles, yielding the total formation of each component as shown in Figure 3b.²⁶ Here, the normally directed N_2 desorption in this figure was shown as the summation

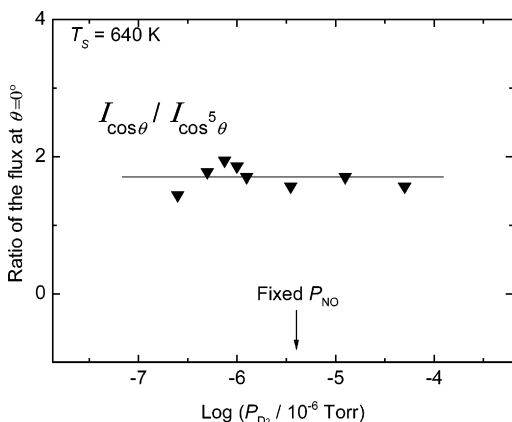


Figure 4. P_{D_2} dependence of the flux ratio of the $\cos \theta$ component to that of the $\cos^5 \theta$ component at $\theta = 0^\circ$. Each flux is designated by $I_{\cos \theta}$ and $I_{\cos^5 \theta}$. These were derived from velocity distribution analysis at $T_s = 640$ K.

including the cosine N_2 component because of the same kinetic behavior as described below. Below the critical pressure, the inclined N_2 desorption and N_2O formation increase with a slope of about 1.5 and slightly decrease in a similar way above it. Furthermore, these components showed a similar T_s dependence.

On the other hand, the N_2 that desorbed along the normal direction increases more rapidly with increasing P_{D_2} below the critical point, remains invariant above it, and decreases rapidly with a further increase. This characteristic became clear at 640 K, where the slope of about 2 was much larger than that for the inclined N_2 desorption and N_2O formation. The ammonia formation became significant only above the critical pressure at 550 K and started at slightly higher D_2 pressure at 640 K.

It should be noticed that the cosine component also increased with increasing D_2 pressure. The AR N_2 signal at the normal direction consisted of the normally directed associative desorption and the thermalized component. Each contribution was separated by velocity distribution analysis, as described in the former subsection. The flux ratio of the $\cos \theta$ component at $\theta = 0^\circ$ to that of the $\cos^5 \theta$ component is shown versus P_{D_2} in Figure 4. It was fairly constant. This constancy was also observed versus the surface temperature.

D. NO + CO Reaction. For a comparison, the AR signals of N-containing products in a steady-state NO + CO reaction are displayed against T_s in Figure 5. All the signals show a tendency similar to that of the signals in the NO + D_2 reaction. The AR N_2 signal at the collimation angle of $\theta = 41^\circ$ increases steeply at around 520 K, is maximized at 550 K, and rapidly decreases at higher temperatures. The N_2O formation follows a similar T_s dependence. On the other hand, the AR N_2 signal at $\theta = 0^\circ$ increases slowly and is maximized at 610 K. The relative N_2 signal at $\theta = 41^\circ$ to that at 0° was sensitive to the P_{NO}/P_{CO} ratio. The normally directed N_2 desorption was enhanced at higher CO pressures. In fact, the critical CO pressure was very close to the NO pressure.²⁷ This situation became clearer in the angular distribution above 600 K. Below 550 K, the N_2 desorption was merely described by the inclined ways, whereas the normally directed component was enhanced at 600 K when $P_{NO}/P_{CO} = 0.5$. This is consistent with the results in the NO + D_2 reaction. The normally directed desorption was enhanced at higher temperatures and higher hydrogen pressures.

The angular distribution at $T_s = 640$ K can be approximated as $0.23 \cos \theta + 0.13 \cos^5 \theta + 0.8\{\cos^{28}(\theta + 41) + \cos^{28}(\theta - 41)\}$. The maximum absolute intensity of the inclined N_2 desorption was almost the same for both reducing reagents. On

the other hand, the normally directed N_2 desorption can be enhanced by hydrogen more than by CO.

IV. Discussion

A. Desorption Components. Four different desorption pathways of N-containing products are operative in a steady-state NO + D_2 reaction on Pd(110). For the N_2 formation, two different pathways work and show different spatial distributions: one is the associative process, which emits N_2 along the surface normal, and the other is due to decomposition of the $N_2O(a)$ intermediate and emits N_2 along 40° off the surface normal in the plane along the [001] direction. In their AR-TPR work of NO + H_2 , Ikai et al. argued that the inclined desorption collimated at 38° was due to the desorption-mediated reaction without passing the intermediate $N_2O(a)$.⁸ In our experiments, however, the N_2 desorption with different collimation angles was assigned to different N_2 formation channels. Ammonia was the main N-containing product at higher P_{D_2} , as reported in the work of Ikai et al., where the H_2 pressure was about 2 orders higher than that of NO.⁸

By state-resolved desorption measurements, Hodgson reported that the N_2 formed in the NO + H_2 reaction on Pd(110) carried considerable vibrational excitation with no excess translational and rotational energy.²⁸ They proposed that N_2 that was formed by the recombination process desorbed via a molecular chemisorption state with an extended N_2 bond. It is difficult to compare their results with ours because of the lack of detailed information regarding the conditions of the experiment. According to our experiments, the apparent translational energy of the products depends on the surface temperature, the NO/ H_2 pressure ratio, and the desorption angle. For example, the thermalized component would contribute mainly to the N_2 desorption at higher T_s and higher H_2/NO pressure ratio for non-angle-resolved measurements.

Recently, Goodman and co-workers reported infrared reflection (IR) spectroscopy work in a steady-state NO + CO reaction on Pd(111), where a possible intermediate of $-NCO(a)$ was proposed according to the absorption signal at around 2255 cm^{-1} .^{29,30} However, this species was not observed below 2×10^{-2} Torr, although the reaction rapidly proceeded even far below this pressure, and no pathways emitting N-containing products were proposed. Unfortunately, the $N_2O(a)$ species giving the absorption in a similar frequency range did not yield a high cross-section for IR absorption compared with $-NCO(a)$. It should be noted that the inclined N_2 emission along about 40° off normal is commonly observed in NO + CO and NO + H_2 reactions on Pd(110). Below about 600 K and at $P_{NO} > P_{CO}$ or P_{H_2} , the N_2 emission is common; on the other hand, at $P_{NO} \ll P_{H_2}$, surface nitrogen is highly converted into NH_3 .

B. Kinetics and Branching. There is a kinetic transition point in the NO + D_2 reaction that is quite similar to that in a NO + CO reaction.²⁷ The overall reaction is mostly controlled by NO dissociation. At hydrogen pressures below the critical value, the surface is fairly covered by NO(a) and O(a). In this region, O(a) has a retarding effect on the NO dissociation. This dissociation or O(a) removal is rate-determining. With increasing hydrogen pressure, the amount of O(a) decreases and the coverage of surface nitrogen increases steeply, which is suggested by the kinetic characteristics described in sections III.C and III.D. However, no hydrogen accumulates on the surface because of the fast H_2O formation and the small heats of adsorption for H_2 and H_2O . This yields increased active (vacant) areas for NO dissociation, and most of N(a) is removed by the reaction with NO(a) via the $N_2O(a)$ intermediate. $N_2O(a)$ is

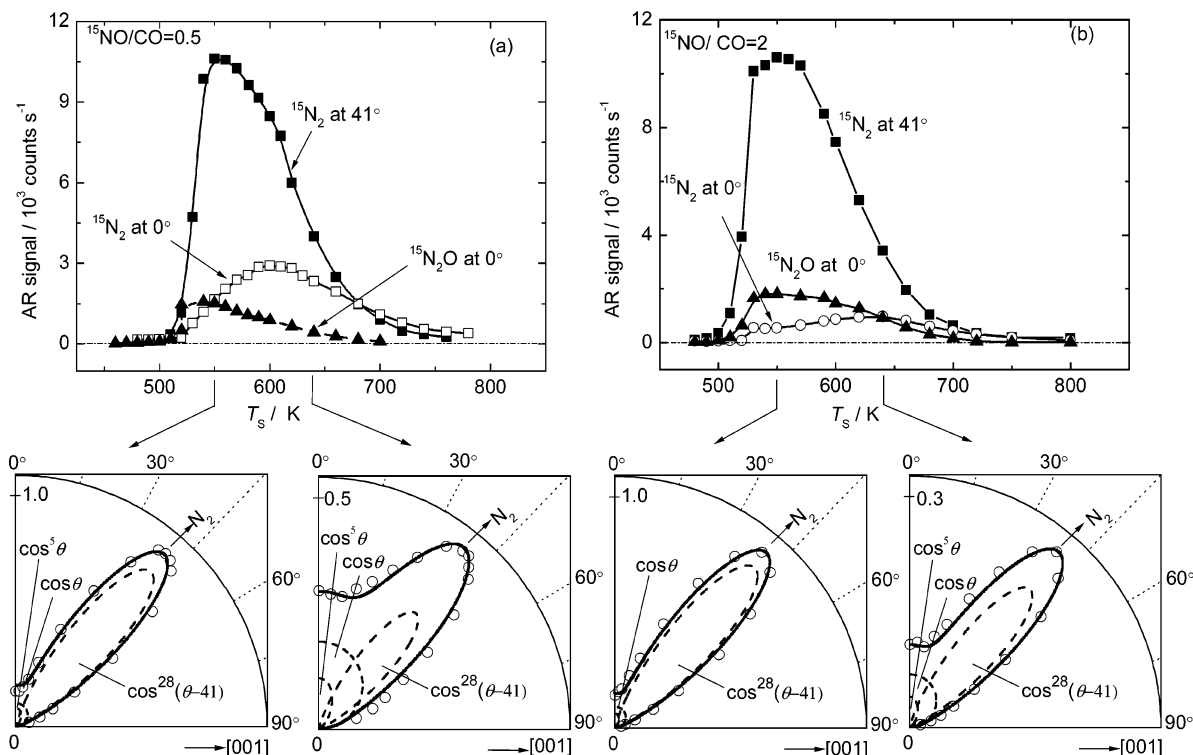


Figure 5. T_s dependence of AR signals of products at their collimation positions in a steady-state $^{15}\text{NO} + \text{CO}$ reaction at $P_{\text{NO}} = 5 \times 10^{-6}$ Torr with $^{15}\text{NO}/\text{CO} =$ (a) 0.5 and (b) 2. Angular distributions of desorbing $^{15}\text{N}_2$ at 550 and 640 K at these $^{15}\text{NO}/\text{CO}$ ratios are also shown. Typical deconvolutions are drawn by broken curves. The ordinate was normalized to the maximum at 550 K.

easily decomposed on vacant parts on Pd(110), emitting N_2 in an inclined way.¹¹ In addition, the reaction rate of the associative $\text{N}(\text{a})$ desorption, process (i), is enhanced more quickly than those of processes (ii) and (iii) since the associative desorption involves two nitrogen atoms, the other processes are coupled with one nitrogen atom and $\text{NO}(\text{a})$, and the amount of $\text{NO}(\text{a})$ does not increase at a fixed NO pressure. This was actually observed in Figure 3. At the critical point, the formation of $\text{O}(\text{a})$ from the NO dissociation is balanced by its removal by $\text{H}(\text{a})$ (or $\text{CO}(\text{a})$ when it is used). Above the critical point, on the other hand, the surface is deficient in $\text{O}(\text{a})$ because of the high hydrogen pressure, and $\text{H}(\text{a})$ can then accumulate, yielding NH_3 . The $\text{N}(\text{a})$ amount decreases slowly with increasing D_2 , keeping a fairly constant N_2 and N_2O formation. This behavior is quite similar to the kinetic switching observed in the CO oxidation.¹⁷ It happens when the product formation step is rapid compared with the supply of reactants on the surface.

The two N_2 formation pathways show different kinetic behavior. The normally directed desorption is favored at higher surface temperatures because the associative process has higher activation energy. In fact, both the formation and decomposition of N_2O have smaller activation energies.^{17,33} The kinetic behavior of the thermalized component (in the $\cos \theta$ form) is always similar to that of the normally directed N_2 desorption (in the $\cos^5 \theta$ form) from process (i), suggesting the formation of both components from a common process; i.e., the branching may take place after the reaction barrier is passed. The lack of the thermalized N_2 component in a steady-state $\text{N}_2\text{O} + \text{CO}$ reaction would support this conclusion. The cosine component showing the desorption after thermalization comes from the associative process. In other words, the product N_2 from process (ii) is not trapped on the surface, and the N_2 from process (i) is largely trapped. From its angular distribution, about 80% of the N_2 from this process was estimated to be trapped above $P_{\text{D}_2} = 1 \times 10^{-6}$ Torr in Figure 3c.²⁶ This is not unreasonable because

a large amount of energy is released in process (ii) due to the formation of the strong O –metal bond.^{17,31} On the other hand, the released energy in process (i) is less because of the strong N –metal bond.³²

Both reactions of $\text{NO} + \text{CO}$ and $\text{NO} + \text{H}_2$ have identical intermediates and common surface-nitrogen removal pathways, showing similar kinetic behavior. A remarkable difference is in the associative process of $\text{N}(\text{a})$, which was more favored in the $\text{NO} + \text{H}_2$ reaction, while the activities for N_2 inclined desorption and N_2O formation were almost the same. This means that more $\text{N}(\text{a})$ can be formed on the surface in a $\text{NO} + \text{H}_2$ reaction. $\text{H}(\text{a})$ can remove $\text{O}(\text{a})$ as quickly as $\text{CO}(\text{a})$, but $\text{H}(\text{a})$ does not accumulate at higher temperatures and shows no retarding effect on the NO dissociation, whereas $\text{CO}(\text{a})$ occupies the surface. Here, the adsorption heat of hydrogen is less than that of CO . A similar observation was reported on $\text{Pt}(100)$ by using synchrotron XPS.³

At higher hydrogen pressures, however, the formation of undesired product ammonia becomes remarkable and the surface may involve NH_X ($X = 1, 2, \text{ or } 3$) species.

C. Velocity Components. The velocity curve after subtraction of the thermalized component is still wide at around 40° as compared with a Maxwellian distribution. The speed ratio (SR) defined as $(\langle v^2 \rangle / \langle v \rangle^2 - 1)^{1/2} / (32/9\pi - 1)^{1/2}$ still had larger values than unity, where v is the velocity of the molecule, $\langle v \rangle$ is the mean velocity, and $\langle v^2 \rangle$ is the mean square velocity. The SR value is unity for a Maxwellian distribution and becomes smaller for distributions of molecules with hyperthermal energy.³⁴ Thus, the distribution after subtraction of the slow component was further deconvoluted into two components by assuming the modified Maxwellian distribution, $f(v) = v^3 \exp\{-(v - v_0)^2/\alpha^2\}$, where v_0 is the stream velocity and α is the width parameter.

Generally, it is difficult to uniquely deconvolute one velocity distribution curve into two distribution curves because two

parameters are required for each distribution on the basis of the modified form. In this case, only three parameters were separately determined by fitting the data points at high- and low-velocity sides. To omit the fourth parameter, we simply assumed a common width parameter.²⁷ The resultant deconvolutions are shown by broken curves in Figure 2b–d. At $\theta = 41^\circ$ where the fast components merely come from the inclined desorption, i.e., almost no contribution from the normally directed component, the faster component shows a translational temperature of 5460–6150 K and the slower one a translational temperature of 2200–2310 K. This result is quite similar to that for the NO + CO reaction on Pd(110).²⁷ The value for the faster component was estimated to be a similar temperature but with an uncertainty of ± 800 K and that for the slower component with an uncertainty of ± 300 K when four parameters were separately adjusted. These fast components were proposed to be due to different vibrational states because of the energy difference close to the vibrational excitation of N₂, 1600 K.¹² This desorption characteristic of desorbing N₂ in the inclined way is common in NO + CO and NO + H₂ reactions. It is not affected by replacement of CO with H₂ as a reducing reagent, supporting the conclusion that the off-normal desorption is due to N₂O(a), which involves neither CO nor hydrogen.

V. Summary

The analysis of both angular and velocity distributions of desorbing products N₂, NH₃, and N₂O has discriminated among four surface nitrogen-removal processes involved in a steady-state NO + H₂ reaction on Pd(110). The pathway through the intermediate N₂O(a) prevails below 600 K and at lower hydrogen pressures, whereas, at high temperatures, the associative desorption of nitrogen adatoms dominates the removal. At high hydrogen pressures, the NH₃ formation becomes major. As compared with CO, hydrogen shows not only a higher reactivity in NO reduction but also a higher selectivity to the associative N₂ desorption.

Acknowledgment. We thank Professor I. Kopal (J. Stefan Institute) for his stimulating discussion. This work was partly supported by a 1996 COE special equipment program of the Ministry of Education, Sports, and Culture of Japan. It was also supported in part by Grant-in-Aid No. 13640493 for General Scientific Research from the Japan Society for the Promotion of Science.

References and Notes

(1) Pãrvulescu, V. I.; Grange, P.; Delmon, B. *Catal. Today* **1998**, *46*, 233.

- (2) De Wolf, C. A.; Nieuwenhuys, B. E. *Catal. Today* **2001**, *70*, 287.
- (3) Rienks, E. D. L.; Bakker, J. W.; Baraldi, A.; Carabini, S. A. C.; Lizzit, S.; Weststrate, C. J.; Nieuwenhuys, B. E. *J. Chem. Phys.* **2003**, *119*, 6245.
- (4) Lombardo, S. J.; Fink, T.; Imbihl, R. *J. Chem. Phys.* **1993**, *98*, 5526.
- (5) Zemlyanov, D. Y.; Smirnov, M. Y.; Gorodetskii, V. V.; Block, J. H. *Surf. Sci.* **1995**, *329*, 61.
- (6) Hallock, A. J.; Matthews, C. M.; Balzer, F.; Zare, R. N. *J. Phys. Chem. B* **2001**, *105*, 8725.
- (7) Colonell, J. I.; Gibson, K. D.; Sibener, S. J. *J. Chem. Phys.* **1996**, *104*, 6822.
- (8) Ikai, M.; Tanaka, K. I. *J. Phys. Chem. B* **1999**, *103*, 8277.
- (9) Ohno, Y.; Kimura, K.; Bi, M.; Matsushima, T. *J. Chem. Phys.* **1999**, *110*, 8221.
- (10) Ohno, Y.; Kopal, I.; Horino, H.; Rzeznicka, I.; Matsushima, T. *Appl. Surf. Sci.* **2001**, *169/170*, 273.
- (11) Horino, H.; Liu, S.; Hiratsuka, A.; Ohno, Y.; Matsushima, T. *Chem. Phys. Lett.* **2001**, *341*, 419.
- (12) Kopal, I.; Kimura, K.; Ohno, Y.; Matsushima, T. *Surf. Sci.* **2000**, *445*, 472.
- (13) Kokalj, A.; Kopal, I.; Matsushima, T. *J. Phys. Chem. B* **2003**, *107*, 2741.
- (14) Horino, H.; Rzeznicka, I.; Matsushima, T.; Takahashi, K.; Nakamura, E. *UVSOR Activity Report (2002)*; Institute for Molecular Science: Okazaki, Japan, 2003; p 209.
- (15) Matsushima, T.; Rzeznicka, I.; Watanabe, K.; Inokuchi, Y.; Ohshimo, K.; Nishi, N. *Nano-technology Support Report 2004*; Institute for Molecular Science: Okazaki, Japan, 2004; p 37.
- (16) Matsushima, T. *Surf. Sci.* **1988**, *197*, L287.
- (17) Matsushima, T. *Surf. Sci. Rep.* **2003**, *52*, 1.
- (18) Kopal, I.; Rzeznicka, I.; Matsushima, T. *Recent Research Developments in Physical Chemistry*; Transworld Research Network: Trivandrum, India, 2002; Vol. 6, p 391.
- (19) Colonell, J. I.; Gibson, K. D.; Sibener, S. J. *J. Chem. Phys.* **1996**, *104*, 6822.
- (20) Ikai, M.; Tanaka, K.-I. *Surf. Sci.* **1996**, *357/358*, 781.
- (21) Ikai, M.; Janssen, N. M. H.; Nieuwenhuys, B. E.; Tanaka, K. I. *J. Chem. Phys.* **1997**, *106*, 311.
- (22) Ikai, M.; Tanaka, K. I. *J. Chem. Phys.* **1999**, *110*, 7031.
- (23) Rzeznicka, I.; Moula, Md. G.; Morales, L.; Ohno, Y.; Matsushima, T. *J. Chem. Phys.* **2003**, *119*, 9829.
- (24) Kobayashi, M.; Tuzi, Y. *J. Vac. Sci. Technol.* **1979**, *16*, 685.
- (25) Rzeznicka, I.; Matsushima, T. *Chem. Phys. Lett.* **2003**, *377*, 279.
- (26) Cao, G.; Moula, Md. G.; Ohno, Y.; Matsushima, T. *J. Phys. Chem. B* **1999**, *103*, 3235.
- (27) Ma, Y.-S.; Rzeznicka, I. I.; Matsushima, T. *Chem. Phys. Lett.* **2004**, *388*, 201.
- (28) Hodgson, A. *Prog. Surf. Sci.* **2000**, *63*, 1.
- (29) Ozensoy, E.; Hess, C.; Goodman, D. W. *J. Am. Chem. Soc.* **2002**, *124*, 8524.
- (30) Ozensoy, E.; Goodman, D. W. *Phys. Chem. Chem. Phys.* **2004**, *6*, 3765.
- (31) Liu, S.; Horino, H.; Kokalj, A.; Rzeznicka, I.; Imamura, K.; Ma, Y.-S.; Kopal, I.; Ohno, Y.; Hiratsuka, A.; Matsushima, T. *J. Phys. Chem. B* **2004**, *108*, 3828.
- (32) Shustorovich, E.; Sellers, E. *Surf. Sci. Rep.* **1998**, *31*, 1.
- (33) Wang, H.; Tobin, R. G.; DiMaggio, C. L.; Fisher, G. B.; Lambert, D. K. *J. Chem. Phys.* **1997**, *107*, 9569.
- (34) Comsa, G.; David, R. *Surf. Sci. Rep.* **1985**, *5*, 145.